Evaporation residue cross sections for ^{32}S $+$ ^{112,116,120,124}Sn from x-ray and direct recoil-nucleus measurements

H. Ernst,* W. Henning, C. N. Davids, W. S. Freeman,† and T. J. Humanic‡

Argonne National Laboratory, Argonne, Illinois 60439

F. W. Prosser and R. A. Racca

University of Kansas, Lawrence, Kansas 66045

(Received 26 August 1983)

Evaporation residue cross sections have been measured for the systems ^{32}S $+$ ^{112,116,120,124}Sn at incident energies between 130 MeV and 247 MeV. Total cross sections were measured by direct detection of recoil nuclei in a particle counter telescope. In addition, total and partial cross sections were determined from K-vacancy production cross sections and K x-ray multiplicities of the evaporation residues. The x-ray multiplicities are of the order of ~ 1 and vary slowly with target mass and incident energy, indicating that x-ray detection can be reliably used to study fusion cross sections induced by heavy projectiles in this mass region. The total evaporation residue cross sections rise with increasing energy, saturate at ~ 190-MeV incident energy, and decrease slightly at higher energies. The saturation value shows distinct differences between systems and ranges from ~ 600 mb for ^{32}S $+$ ^{112}Sn to ~ 800 mb for ^{32}S $+$ ^{124}Sn. The gross behavior of the partial evaporation residue cross sections is in agreement with statistical model calculations, but there remain deviations in the element distribution of the evaporation residues which might be explained by contributions from incomplete fusion reactions. As a byproduct we have measured K-vacancy production cross sections for atomic excitation of the target atoms by the projectiles and compared them with theoretical predictions.

NUCLEAR REACTIONS ^{32}S $+$ ^{112,116,120,124}Sn, evaporation residue cross sections $\sigma(E,\theta)$ and $\sigma(E,Z)$, K x-ray cross sections and multiplicities; statistical model calculations.

I. INTRODUCTION

In this paper we report on extensive studies of complete fusion reactions of ^{32}S $+$ ^{112,116,120,124}Sn at incident energies between 130 and 247 MeV. Our objective was to investigate the conditions for compound nucleus formation and its survival probability against fission, which gradually becomes the major decay channel for heavy compound nuclei formed in this mass and energy region. In particular, the choice of targets that differ by as much as 12 neutrons allows the study of the particle evaporation-to-fission branching ratio as a function of the neutron excess of the compound nucleus under similar entrance channel conditions. In addition, limitations on compound nucleus formation of heavy systems due to increases in fusion threshold energies as predicted in dynamical fusion-model calculations[1] and, on the other hand, experimental indications of enhanced sub-barrier fusion cross sections for heavier systems[2] are strong motivations to perform detailed studies of heavy-ion compound nuclear reactions in the mass region of $A \approx 150$ and heavier.

The direct detection of evaporation residues (ER), formed by light particle evaporation from the compound nucleus, becomes increasingly difficult with increasing mass when conventional methods like ΔE-E and time of flight are used. One approach to solve those experimental

difficulties is the use of a recoil spectrometer such as a velocity filter[3,4] or an electrostatic separator.[5]

In a different approach which we used in this work, one can identify the ER through the detection of their prompt characteristic x rays[6-18] which originate mainly from converted γ transitions deexciting the compound nucleus. The contribution of atomic processes to the ER x-ray yield is small and can be neglected for heavy and asymmetric systems.[6,10] Besides its greater simplicity, a conceptual advantage of the x-ray method over the use of spectrometers with transit times of typically microseconds are the short K x-ray lifetimes of 10^{-15}–10^{-17} sec, which in principle allow the study of very-short-lived compound nuclei. In addition, because of the high energy resolution which can be obtained with x-ray detectors, a unique Z identification of the ER can be achieved.

To relate the K x-ray production cross sections to the ER cross sections, the K x-ray multiplicity $\langle M_K \rangle$, i.e., the average number of x rays produced per fusion event, must also be measured. This can be accomplished by x-ray—x-ray coincidence measurements or directly by comparing the x-ray production cross sections with the total ER cross section measured independently using a conventional method, e.g., a particle ΔE-E telescope. In order to study the prospects of the x-ray technique we used both approaches, though, in future applications and especially for

heavier systems, one would like to obtain this information from x-ray measurements alone. Since the x-ray multiplicities are sensitive to the energies and multiplicities of the involved electromagnetic transitions, they also may provide information on nuclear structure effects[11−13] such as changes in nuclear shape.

In the following sections we first describe the experimental methods and then give an interpretation of the results in the framework of the liquid-drop and statistical model. The possibility of precompound light particle emission is also discussed. Finally, some aspects of the characteristic x rays emitted by atomic excitation of the target atoms will be mentioned. A partial account of the present study has been published in a recent letter.[18]

II. X-RAY MEASUREMENTS

In our x-ray experiments we used enriched ($>99\%$) ^{116,120,124}Sn targets with thicknesses ranging from 110 to 570 $\mu g/cm^2$ on 10-$\mu g/cm^2$ carbon backings. ^{32}S^{13+} beams in the energy range of 130—202 MeV with an intensity of typically 20 charge nA were provided by the Argonne tandem-superconducting linac accelerator. For the on-line data recording a PDP 11/45 computer was used.

For the x-ray singles and the x-ray—x-ray coincidence measurements we used two planar Si(Li) detectors with 300 mm^2 and 80 mm^2 active area, 3 mm thickness, and 250 eV resolution at 6-keV x-ray energy. The detectors were placed at $+90°$ and $-90°$ with respect to the beam direction at a distance of 29 mm from the target, which was rotated by 45°, thus increasing the effective target thickness by a factor of 1/cos(45°).

In order to reduce the very strong characteristic x-ray yield produced by atomic excitation of the Sn targets, we placed absorbers consisting of 2.4-mm Lucite and 6.4-mm aluminum between detectors and target. The Sn x-ray yield [$E(K\alpha_1)=25.3$ keV] was thus reduced by a factor of 22, while the ER K x rays [$E(K\alpha_1)=46$ keV for $Z=66$] were attenuated by only a factor of ~ 2.

The absolute and relative efficiencies of the detectors with the absorbers in front of them were measured with radioactive sources of known activity placed at the target position. The accuracy of this calibration is estimated to be 8%. Figure 1 shows a representative in-beam x-ray spectrum. In spite of the attenuation by the absorbers, the characteristic target x rays were still more intense than the ER x rays by over two orders of magnitude. In Fig. 2 we have plotted the region of the ER x rays for some selected systems. Only the energy region of the $K\alpha$ x rays is shown. The ER $K\beta$ x rays are very weak (Fig. 1) and may also be contaminated by pileup events of the intense Sn target x rays which would appear exactly in the energy region of the ER $K\beta$ x rays. For this reason they were not used in our analysis. The ER populated in this experiment are in the region of the rare-earth nuclei, which is very favorable for $K\alpha$ x-ray spectroscopy, since the energy difference between the x rays of neighboring Z elements is large enough for an easy separation but does not yet produce overlap of the $K\alpha_1$ line of one element with the $K\alpha_2$
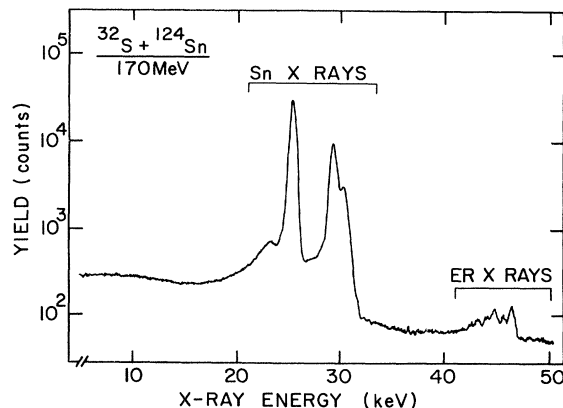

FIG. 1. X-ray spectrum for ^{32}S+^{124}Sn at 170-MeV incident energy. The target x rays and the evaporation residue x rays are indicated.

line of the next, as in the case for heavier nuclei.

In Fig. 2 one already observes the qualitative feature that charged particle (proton and alpha particle) evaporation plays a prominent role in the present systems, and indeed dominates in situations where the evaporation residue strength moves to very proton-rich nuclei, either as a consequence of lower neutron number of the target nucleus (^{116}Sn as compared to ^{124}Sn in Fig. 2) or, for a fixed target nucleus, as a consequence of higher incident energy and more light-particle evaporation. For a more quantitative analysis, x-ray yields were obtained by least-squares fits of a sum of symmetric Gaussian lines on a linear background, to the measured x-ray spectra as illustrated in Fig. 3. For absolute and relative normalization we mea-
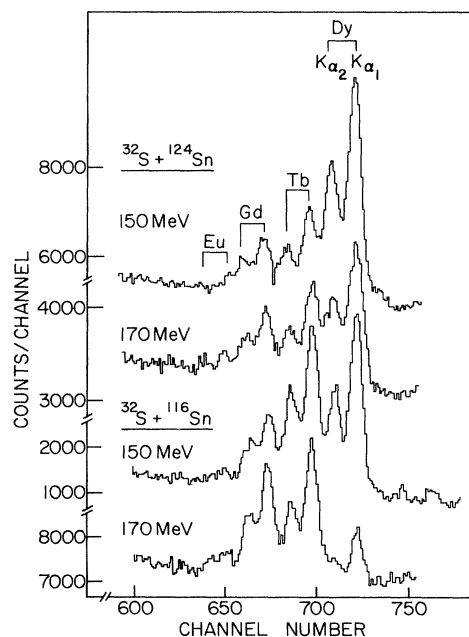

FIG. 2. Evaporation residue $K\alpha$ x-ray spectra for the reaction ^{32}S+^{116,124}Sn at 150- and 170-MeV incident energies. The compound nucleus is ^{148,156}Dy ($Z=66$). The $K\beta$ x rays, appearing at higher energies, are not shown.
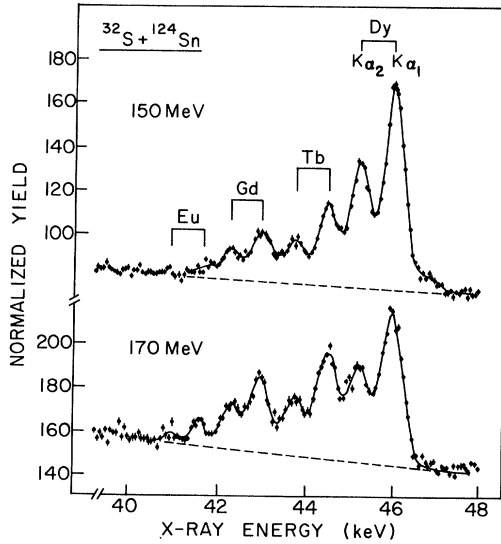
FIG. 3. Evaporation residue $K\alpha$ x-ray spectra for the reaction $^{32}S+^{124}Sn$ at 150- and 170-MeV incident energies. The solid lines are the results of least-squares fits of a sum of symmetric Gaussian lines superimposed over a linear background indicated by the dashed lines.

sured the yield N_M of elastically scattered beam particles with a silicon surface barrier monitor detector placed at 6.5° and subtending a solid angle of $\Omega_M=0.09$ msr. Independent checks of the normalization were done by means of a calibrated Faraday cup and by comparison of the evaporation residue $K\alpha$ x-ray yields N_K with the characteristic Sn x-ray yields measured at the same time. The total error of the normalization procedure is estimated to be $\sim 10\%$. Absolute K-vacancy production cross sections σ^K were derived from the expression

$$\sigma^K = \frac{N_K T_K}{\omega_K \epsilon_K} \frac{K\alpha + K\beta}{K\alpha} \frac{\sigma_M^R \Omega_M}{N_M T_M} \; . \tag{1}$$

Here, σ_M^R is the Rutherford cross section at $\theta=6.5°$, T_K and T_M are dead-time correction factors, ϵ_K is the x-ray detector efficiency including solid angle, ω_K is the K-shell luminosity[19] ($\omega_K=0.93$ for $Z=66$) and $(K\alpha+K\beta)/K\alpha$ is derived from the known $K\alpha/K\beta$ intensity ratios.[19] Since ω and the ratio $K\alpha/K\beta$ are valid, in principle, only for atomic ground-state configurations, their use for highly excited ions may introduce an additional uncertainty (see also Sec. IV D). The total systematic error is therefore estimated to be of the order 15—20%. The results for the total and partial K-vacancy production cross sections, σ_{tot}^K and σ_{Z-i}^K, are listed in Table I. Z denotes the atomic number of the compound nucleus and the index i counts how many units of charge are carried away by charged-particle evaporation. In Fig. 4, the K-vacancy production cross sections are plotted versus the center-of-mass energy $\bar{E}_{c.m.}$ corrected for energy loss of the projectile in the target.

In order to determine total and partial K x-ray multiplicities $\langle M_K \rangle$, i.e., the average number of K x-rays emitted per fusion event, we recorded x-ray—x-ray coincidences

for ^{116}Sn and ^{124}Sn at 150 and 170 MeV in extended runs of ~ 6 h. The multiplicities are derived from the ratio of singles to coincidence count rate in the following way: The count rate N_1 in x-ray detector 1 is

$$N_1 = C\langle M_K \rangle \frac{d\sigma}{d\Omega} \epsilon_1 \; , \tag{2}$$

where ϵ_1 is the detector efficiency including the solid angle, $d\sigma/d\Omega$ is the differential fusion cross section, and C is a constant depending on beam intensity and target thickness. A corresponding expression holds for the count rate N_2 in the second x-ray detector. The coincidence rate N_{12} is then given by
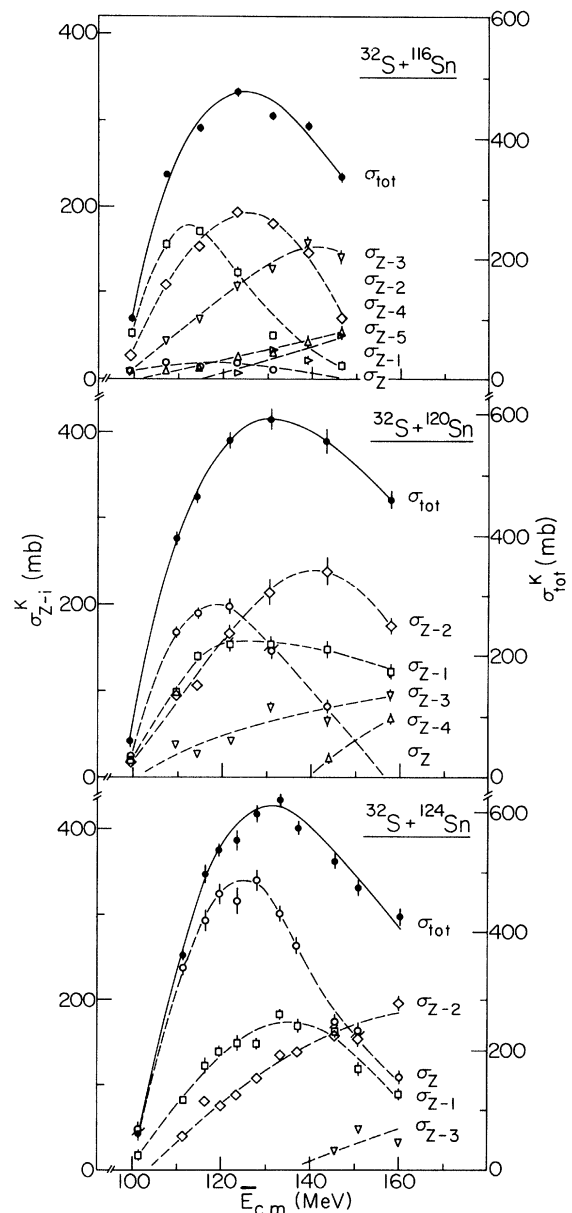

FIG. 4. Total (σ_{tot}^K) and partial (σ_{Z-i}^K) K-vacancy production cross sections as a function of center-of-mass energy $\bar{E}_{c.m.}$, corrected for energy loss of the projectile in the target.

TABLE I. Partial (σ_{Z-i}^K) and total (σ_{tot}^K) K-vacancy production cross sections for the reactions ^{32}S+^{116,120,124}Sn as deduced from the evaporation residue x-ray measurements. The index i in σ_{Z-i}^K counts how many units of charge were carried away by light particle evaporation from the compound nuclei ^{148,152,156}Dy with atomic number $Z=66$. The center-of-mass energies $\bar{E}_{\text{c.m.}}$ are corrected for energy loss of the projectile in the target. The last column contains the total K-vacancy multiplicity $\langle M_K \rangle = \sigma_{\text{tot}}^K/\sigma^{\text{ER}}$. All quoted errors contain statistical uncertainties only. An additional systematic error of $\sim 15\%$ due to absolute normalization and detector-efficiency calibration should be added.

Target	E_{lab} (MeV)	$\bar{E}_{\text{c.m.}}$ (MeV)	σ_Z^K (mb)	σ_{Z-1}^K (mb)	σ_{Z-2}^K (mb)	σ_{Z-3}^K (mb)	σ_{Z-4}^K (mb)	σ_{Z-5}^K (mb)	σ_{tot}^K (mb)	$\langle M_K \rangle$
^{116}Sn	130.0	99.5	8±3	53±4	29±4	9±3			99±8	1.10±0.12
	140.0	107.4	20±3	157±5	109±4	45±2	10±2		341±7	1.21±0.11
	150.0	115.3	16±2	162±4	155±4	70±3	14±2		417±7	0.97±0.08
	160.0	123.3	19±3	124±5	193±6	108±5	27±4	7±3	478±11	0.89±0.07
	170.0	131.0	12±2	52±3	181±4	128±3	31±2	34±2	438±7	0.71±0.06
	180.0	139.0		45±4	148±6	160±6	44±4	23±4	420±11	0.66±0.06
	190.0	146.8		16±4	72±5	142±8	56±5	52±5	338±12	0.52±0.04
^{120}Sn	130.0	99.6	21±5	19±4	19±4				59±8	0.84±0.13
	141.0	109.6	167±7	99±4	94±4	38±3			398±9	1.08±0.08
	146.8	114.2	190±7	140±5	107±4	26±3			463±10	1.01±0.06
	156.0	121.5	198±10	154±8	165±8	41±3			558±14	1.03±0.06
	168.0	131.0	145±8	153±9	215±12	81±5			594±17	0.91±0.06
	183.7	143.4	82±7	148±11	239±16	66±7	22±6		557±21	0.75±0.06
	202.0	157.9		122±8	175±9	95±7	67±6		459±15	0.63±0.04
^{124}Sn	130.0	101.5	45±6	17±5	40±3				62±8	0.67±0.12
	141.0	111.6	238±8	82±4	81±5				360±9	0.75±0.07
	146.8	116.2	293±12	123±8	75±3				497±14	0.87±0.05
	151.0	119.5	324±9	139±5	88±4				538±9	0.85±0.05
	156.0	123.5	315±16	149±8	109±5				552±16	0.81±0.05
	161.5	127.9	341±12	148±6	137±4				598±13	0.82±0.05
	168.0	133.1	302±8	182±5	138±5				621±9	0.81±0.05
	173.0	137.1	264±9	169±7	158±6	23±4			571±12	0.72±0.05
	183.7	145.6	174±7	162±6	155±9	48±4			517±12	0.64±0.04
	190.3	150.8	153±9	119±7	196±9	32±4			475±14	0.58±0.04
	202.0	160.2	110±7	89±6					427±14	0.53±0.03

TABLE II. Multiplicities $\langle M_K \rangle$ for 150- and 170-MeV ^{32}S ions incident on ^{116}Sn and ^{124}Sn targets, derived from the x-ray—x-ray coincidence measurements. Columns 3—5 contain the partial multiplicities for different evaporation residues, which are indicated by $Z-i$, where Z denotes the compound nucleus atomic number and the index i counts how many units of charge are carried away by light-particle evaporation. In the last column, the weighted averages are listed.

Target	E_{lab} (MeV)	Z	$Z-1$	$Z-2$	$Z-3$	$Z-4$	Average
^{116}Sn	150		1.22±0.14	1.40±0.15	1.27±0.27	0.99±0.37	1.25±0.15
^{116}Sn	170		0.81±0.19	0.70±0.10	0.50±0.08	1.16±0.23	0.72±0.11
^{124}Sn	151	1.06±0.17	0.71±0.21	1.59±0.45	1.26±0.52		1.07±0.14
^{124}Sn	168	0.78±0.20	1.78±0.32	1.03±0.43			0.99±0.43

$$N_{12} = \left\langle CM_K \frac{d\sigma}{d\Omega} \epsilon_1 \left[\frac{\epsilon_2}{4\pi}(M_K - 1) \right] \right\rangle . \quad (3)$$

The term in square brackets is the probability of observing a K x ray within the averaging time window in detector 2 under the condition that a K x ray was observed in detector 1. The multiplicity is now derived as

$$\frac{N_{12}}{N_1} \frac{4\pi}{\epsilon_2} = \frac{\langle M_K(M_K - 1)\rangle}{\langle M_K \rangle}$$

$$= \langle M_K \rangle + \frac{\Delta^2}{\langle M_K \rangle} - 1 = \langle M_K \rangle . \quad (4)$$

The last equal sign holds exactly only for a Poisson distribution, in which case the variance $\Delta^2 = \langle M_K^2 \rangle - \langle M_K \rangle^2$ is equal to $\langle M_K \rangle$. To what extent this condition is fulfilled will be discussed in Sec. IV. The total and partial multiplicities are calculated with Eq. (4) using dead-time corrected yields with the background subtracted, i.e., less the accidental coincidences and coincidences with Compton-scattered higher-energy γ rays. The results are listed in Table II. The total number of coincidence counts was only 200—300 in each run, the main limitation being the rather small active areas of the x-ray detectors being used.

As a by-product, we also measured the target K-vacancy production cross sections σ_{Sn}^K due to atomic excitation of the Sn target atoms by the projectile. In this case both the $K\alpha$ and $K\beta$ x rays were measured, which allows a comparison of the experimental $K\alpha/K\beta$ ratios with the known values for the ground-state configuration. The K-vacancy production cross sections σ_{Sn}^K were derived from the expression

$$\sigma_{\text{Sn}}^K = \left[\frac{N_{K\alpha}}{\epsilon_{K\alpha}} + \frac{N_{K\beta}}{\epsilon_{K\beta}} \right] \frac{T_K}{\omega_K} \frac{\sigma_M^R \Omega_M}{N_M T_M} \quad (5)$$

and are listed in Table III together with the deduced $K\alpha/K\beta$ ratios. In Figs. 5 and 6 σ_{Sn}^K and $K\alpha/K\beta$ are plotted versus $\bar{E}_{\text{lab}}/A$ where $\bar{E}_{\text{lab}}$ is the incident projectile energy corrected for energy loss in the target and A is the projectile mass. $N_{K\alpha}$ and $N_{K\beta}$ are the Sn($K\alpha$) and Sn($K\beta$) x-ray yields. Since the experiment was not optimized for the detection of Sn x rays, the efficiencies for the $K\alpha$ and

$K\beta$ Sn x rays, $\epsilon_{K\alpha}$ and $\epsilon_{K\beta}$, are rather small and quite different from each other due to the steep slope of the efficiency curve at those energies. This increases the uncertainty in the absolute normalization to $\sim 20\%$.

TABLE III. K vacancy production cross sections σ_{Sn}^K and $K\alpha/K\beta$ intensity ratios derived from the target x rays emitted in the reactions ^{32}S + ^{116,120,124}Sn. For the luminosity $\omega = 0.84$ was used. The laboratory energies $\bar{E}_{\text{lab}}$ are corrected for energy loss of the projectile in the target. The statistical errors are $\sim 1\%$ and reflect the relative uncertainties as a function of energy and between targets; a systematic error of $\sim 20\%$ due to normalization and detector-efficiency calibration should be added for absolute uncertainties.

| Target	E_{lab} (MeV)	$\bar{E}_{\text{lab}}/A$ (MeV/u)	σ_{Sn}^K (b)	$K\alpha/K\beta$
^{116}Sn	130.0	3.97	52	3.73
	140.0	4.29	73	3.66
	150.0	4.60	101	3.57
	160.0	4.92	132	3.51
	170.0	5.23	168	3.45
	180.0	5.55	195	3.38
	190.0	5.86	211	3.31
^{120}Sn	130.0	4.00	53	3.74
	141.0	4.34	81	3.64
	146.8	4.52	95	3.60
	156.0	4.81	124	3.53
	168.0	5.19	159	3.45
	183.7	5.68	204	3.35
	202.0	6.26	251	3.25
^{124}Sn	130.0	4.05	59	3.72
	141.0	4.40	86	3.63
	146.8	4.58	99	3.58
	151.0	4.71	113	3.55
	156.0	4.86	131	3.50
	161.5	5.04	147	3.48
	168.0	5.24	169	3.44
	173.0	5.40	180	3.39
	183.7	5.73	209	3.34
	190.3	5.94	230	3.31
	202.0	6.30	255	3.27
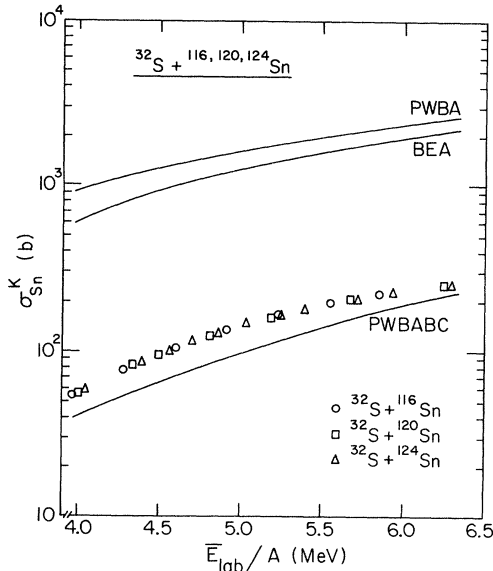
FIG. 5. K-vacancy production cross sections σ_{Sn}^K for atomic excitation of the Sn target atoms by the ^{32}S projectile as a function of $\bar{E}_{lab}/A$. The solid lines are theoretical predictions which are explained in the text.

III. MEASUREMENT OF EVAPORATION RESIDUES WITH A PARTICLE TELESCOPE

For the direct measurements of the ER we used thin ^{112,116,120,124}Sn targets of 100—150 μg/cm^2 areal density on 10-μg/cm^2 carbon backings. ^{32}S^{13+} beams in the energy range 130—247 MeV were provided by the Argonne tandem superconducting linac. Evaporation residues were detected at forward angles between $\theta_{lab}=1°$ and $11°$ in a 165 cm diam scattering chamber with a ΔE-E telescope subtending a solid angle of 5.9×10^{-6} sr and consisting of a 3.6 μm,ΔE, and a 300 μm,E, silicon surface barrier detector. The 0° position of the detector arm was determined within $\pm0.02°$ by forward angle elastic scattering

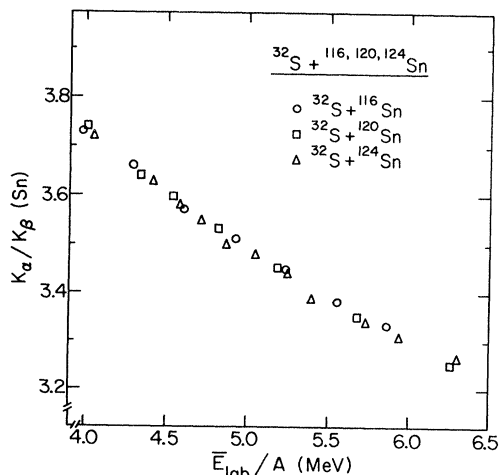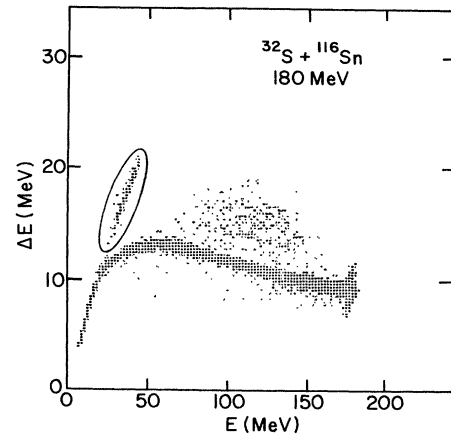FIG. 6. $K\alpha/K\beta$ x-ray intensity for the target x rays as a function of $\bar{E}_{lab}/A$.

FIG. 7. Two-dimensional ΔE vs E particle spectrum for the reaction 180-MeV ^{32}S+^{124}Sn at $\theta_{lab}=3°$. The evaporation residues are encircled.

measurements on both sides of the beam. In addition to a calibrated beam current integrator two silicon detectors placed at $+10°$ and $-10°$ were used to monitor the beam direction and the product of target thickness times beam flux.

Figure 7 shows an example of a two-dimensional spectrum in the energy-loss ΔE versus total-energy E plane. The ER formed in the ^{32}S + Sn reactions are well separated from the low-energy tail of the beam particles and from the reaction products of the beam with the carbon backing, appearing as a distinct group between 80 and 150 MeV total energy. The yield within the encircled region in the ΔE-E spectrum in Fig. 7 was integrated to determine the ER yield. Angular distributions in the range $1°\leq\theta\leq11°$ were measured at two selected energies (Fig. 8).

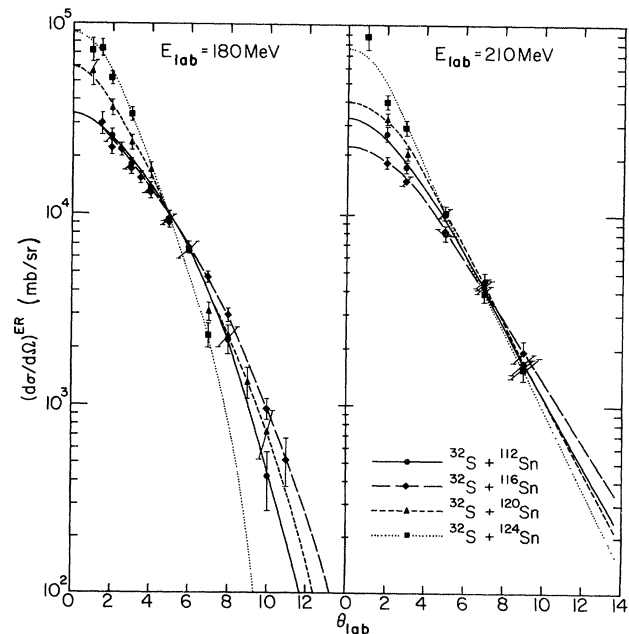FIG. 8. Differential cross sections $d\sigma/d\Omega$ as a function of laboratory angle θ_{lab} for ^{32}S+^{112,116,120,124}Sn evaporation residues as measured with the ΔE-E particle telescope.

TABLE IV. Evaporation residue cross sections σ^{ER} for $^{32}S + {}^{112,116,120,124}Sn$ as measured with the ΔE-E telescope. The energies at which full angular distributions were recorded are marked with an asterisk. The quoted errors include statistical uncertainties only. The total uncertainties, which include the normalization errors, are $\sim 15\%$.

	^{112}Sn		^{116}Sn		^{120}Sn		^{124}Sn	
E_{lab} (MeV)	$E_{c.m.}$ (MeV)	σ^{ER} (mb)	$E_{c.m.}$ (MeV)	σ^{ER} (mb)	$E_{c.m.}$ (MeV)	σ^{ER} (mb)	$E_{c.m.}$ (MeV)	σ^{ER} (mb)
140	108.9	317±30	109.7	279±28	110.5	279±29	111.3	478±46
160	124.4	417±33	125.4	565±41	126.3	615±43	127.2	768±50
180*	140.0	596±42	141.1	636±33	142.1	715±36	143.1	752±50
185	143.9	641±44	145.0	691±42	146.1	703±41	147.1	774±54
190	147.8	599±39	148.9	693±48	150.0	762±54	151.0	845±53
200	155.6	585±39	156.8	634±27	157.9	725±42	159.0	766±52
210*	153.3	586±30	164.6	604±40	165.8	729±47	166.9	763±48
220	171.1	568±40	172.4	565±30	173.7	650±35	174.9	720±45
230	178.9	558±33	180.3	579±39	181.6	636±41	182.8	769±50
240	186.7	482±28	188.1	563±26	189.5	639±31	190.8	703±40
247	192.1	471±29	193.6	523±28	195.0	599±32	196.3	692±39

σ^{ER} was determined by numerically integrating these angular distributions. The largest contributions to the angle-integrated evaporation residue cross sections come from angles around $\theta_{lab} = 3°$ as demonstrated in Fig. 9, where the differential cross section is multiplied by the solid-angle element $2\pi\sin\theta$. In addition, single-angle measurements at $\theta_{lab} = 3°$ were used, with linear corrections to account for the energy dependence of the angular distributions, to determine cross-section values at other energies. The relative normalization at energies with single-angle measurements was provided by the monitor detectors. The yield of elastically scattered ^{32}S ions detected *simultaneously* with the evaporation residues was used to establish the absolute normalization of σ^{ER}. The uncertainty in the absolute ER cross sections introduced by the normalization procedures is estimated to be of the order of 10%. The resulting fusion cross sections are listed in Table IV and graphed in Fig. 10. The curves are smooth averages through the data points and at the lowest energies reflect the behavior observed near the barrier by Beier *et al.*[20]

IV. DISCUSSION

A. Total evaporation residue cross sections

The ER cross sections, σ^{ER}, are smooth functions of the incident energy. σ^{ER} saturates for all targets near $E_{c.m.} \approx 150$ MeV ($E_{lab} \approx 190$ MeV), with increasingly higher maximum cross-section values for increasing target neutron number, ranging from ~ 600 mb for $^{32}S + {}^{112}Sn$ to ~ 800 mb for $^{32}S + {}^{124}Sn$. σ^{ER} decreases slightly towards higher energies; this falloff is more pronounced for the more neutron-deficient compound nuclei.

The choice of Sn targets that differ by as much as 12 neutrons provides us with measurement of the ER cross sections as a function of neutron number under similar entrance channel conditions. In Table V we have listed the saturation evaporation residue cross sections σ^{ER}_{sat}, critical

angular momenta l_{cr}^{ER} derived from $\sigma = \pi \lambda^2 (l + 1)^2$, and compound nucleus excitation energies E^* at 190 MeV incident energy. The last column contains the intrinsic target nuclear quadrupole moments Q_0 derived from the $B(E2, 0^+ \rightarrow 2^+)$ values according to the formula $Q_0 = [B(E2)5/16\pi]^{1/2}$. Owing to the similarity of the
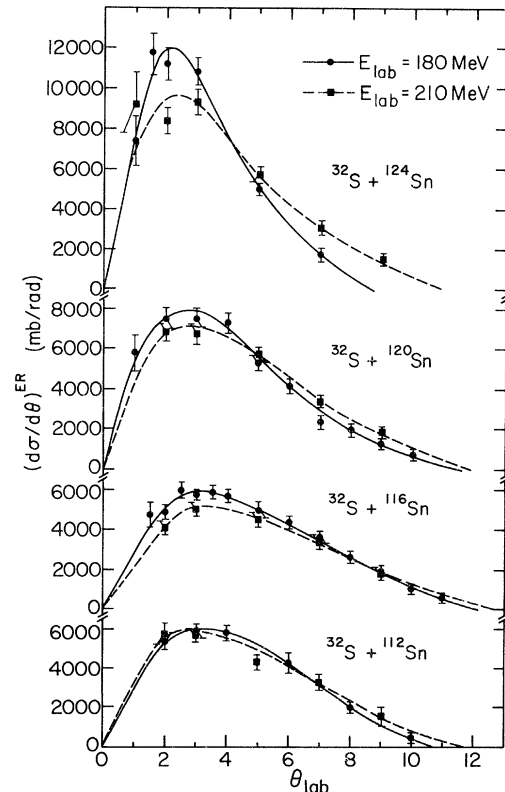

FIG. 9. Angular distributions for the $^{32}S + {}^{112,116,120,124}Sn$ evaporation residues in terms of $d\sigma/d\theta = 2\pi(d\sigma/d\Omega)\sin\theta$ so that the area under the curves is the angle-integrated cross section.
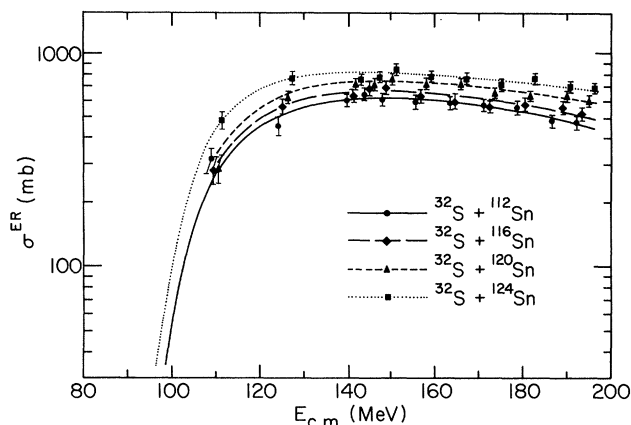
FIG. 10. Evaporation residue cross sections σ^{ER} for ^{32}S$+^{112,116,120,124}$Sn as a function of center-of-mass energy. The lines are drawn to show the smooth average behavior of the excitation functions and to mark the characteristic differences in cross section magnitudes between the different targets. At low incident energies the lines indicate the cross section behavior experimentally observed by Beier et al. (Ref. 20).

ground-state structure for the different Sn target nuclei, evidenced by the essentially identical values of Q_0, we do not expect entrance channel effects to produce noticeable differences in the fusion cross sections. On the other hand, the angular momenta reached in the present reactions approach those predicted to have vanishing fission barriers in the rotating liquid drop model[21]: $l(B_f=0)\approx95\hbar$ and $l(B_f=8$ MeV$)\approx77\hbar$, where B_f is the fission barrier height. Consequently, the differences in evaporation residue cross sections most likely result from differences in fission probability for otherwise identical fusion cross sections. Indeed, we have measured the distribution of reaction strength, including fission and deep-inelastic processes at high incident energy ($E_{lab}=247$ MeV) and find that fission and evaporation residue cross sections add up to a constant value for the different Sn targets. A detailed discussion of these results will be presented in a forthcoming publication.[22] Here we simply note that the qualitative behavior of a decrease in ER cross section with neutron deficit is consistent with a decrease in fission barrier height and, as a consequence, an increase in fission decay probability.

TABLE V. Saturation evaporation residue cross sections σ_{sat}^{ER}, critical angular momenta l_{cr} derived from $\sigma=\pi\lambdabar^2(l+1)^2$, and compound nucleus excitation energies E^* at 190-MeV incident energy. The last column contains the static intrinsic target nuclear quadrupole moments Q_0 derived from the $B(E2,0^+\rightarrow2^+)$ values with the formula $Q_0=[B(E2)5/16\pi]^{1/2}$.

Target	σ_{sat}^{ER} (mb)	l_{cr} ($\hbar$)	E^* (MeV)	Q_0 (b)
^{112}Sn	605±29	57	55.8	1.65±0.37
^{116}Sn	664±27	61	67.2	1.46±0.17
^{120}Sn	726±31	64	71.3	1.49±0.15
^{124}Sn	784±37	67	76.2	1.47±0.16

B. X-ray multiplicities

As described in Sec. II, the K x-ray multiplicities $\langle M_K \rangle$ were derived from x-ray—x-ray coincidences and singles in a way [Eq. (4)] that depends on the assumption that the x-ray multiplicity distribution averaged over all decay paths follows a Poisson distribution. This seems to be a rather limiting assumption. However, following arguments from Ref. 13, where a detailed discussion of the statistical characteristics of x-ray multiplicities is given, we might expect that the errors which result from deviations from a Poisson distribution are indeed tolerable. For a single γ-decay path, any x-ray multiplicity distribution that is not Poisson but has the same mean $\langle M_K \rangle$ would result[13] in $\Delta^2/\langle M_K \rangle < 1$ in Eq. (4). Thus by using Eq. (4) one tends to underestimate the actual multiplicity. On the other hand, if one averages over several decay paths, as we definitely do by averaging over various final reaction products, and if the average multiplicity differs among the constituents, then the distribution averaged over various decay paths is broader than a Poisson distribution. This is true even if the distribution is Poisson for each constituent. Overall, the two effects tend to counteract. The authors of Ref. 13 estimate that in a situation similar to the present one can put a limit of ±0.2 on the systematic error for the deduced multiplicities.

In the present study we can test the assumptions made above by comparing the multiplicities derived from the coincidence experiment with those directly determined from the ratio of K-vacancy production cross section σ^K to ER cross section σ^{ER} as measured with the particle telescope. The multiplicity determined from evaporation residue and x-ray singles cross sections, summed over all channels i, is given by the expression

$$\langle M \rangle_{ER-x} = \frac{\sum_i \sigma_i^{ER}\langle M_i \rangle}{\sum_i \sigma_i^{ER}} \qquad (6)$$

whereas the averaged multiplicity determined from x-ray singles and coincidences (already assuming a Poisson multiplicity distribution for individual decay channels) is given by

$$\langle M \rangle_{x-x} = \frac{\sum_i \sigma_i^{ER}\langle M_i \rangle\langle M_i \rangle}{\sum_i \sigma_i^{ER}\langle M_i \rangle} . \qquad (7)$$

One verifies that always $\langle M \rangle_{ER-x} \le \langle M \rangle_{x-x}$. Since our particle measurements do not resolve evaporation residues of different Z (and in principle cannot, due to the overlap of the energy loss curves for recoil nuclei of the mass and recoil energy observed here; which is, of course, the reason why we have studied the compound nuclear x rays), a comparison is only possible for the averaged multiplicities determined from Eqs. (6) and (7).

The results for $\langle M_K \rangle_{ER-x}=\sigma^K/\sigma^{ER}$ are listed in the last column of Table I and plotted in Fig. 11 together with the values for $\langle M_K \rangle_{x-x}$ as derived from the coincidence experiment. From Fig. 11 we find that the two agree quite
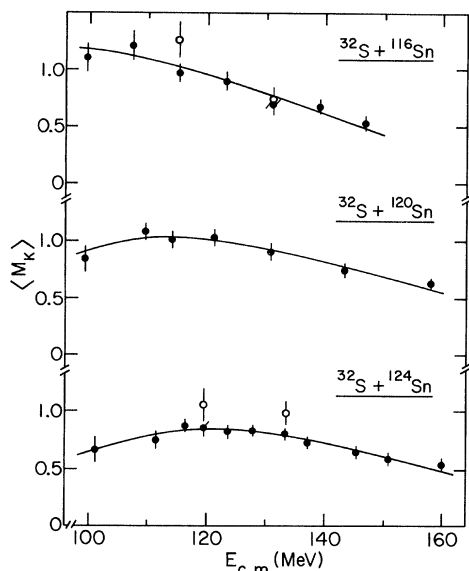
FIG. 11. Total K x-ray multiplicities $\langle M_K \rangle$ for $^{32}S + ^{116,120,124}Sn$ as derived from the ratio of the K-vacancy production cross sections to total evaporation residue cross sections (solid dots) vs center-of-mass energy. The values of $\langle M_K \rangle$ derived from the x-ray—x-ray coincidence measurements are indicated as open circles. The lines are drawn to show the smooth energy dependence of $\langle M_K \rangle$.

well. This may not be too surprising in light of what was stated above, and also because in reality fewer channels might contribute to the averaging than first expected. First, if we consider an individual element (Z) of the evaporation residues, we generally expect that at a given incident energy one isotope dominates due to the systematics of xn-neutron evaporation. Considering the average over several Z's, we find from Fig. 4 that at most bombarding energies one or two, at most three, Z channels dominate. For one decay path, Eqs. (6) and (7) are identical; for two or three channels the averaging procedure yields close values for both equations provided the individual multiplicities are not too drastically different.

From the behavior observed for systems formed with lighter projectiles[11–15] this latter assumption may not seem reasonable. For example, for the ^{124}Sn target at our lowest incident energy neutron evaporation is by far the strongest decay channel and the populated Dy nuclei are expected to be the same as those studied in ^{12}C and α-induced reactions[15] by Chmielewska *et al.* They found multiplicities similar to ours, but in general somewhat smaller and showing an odd-even staggering between isotopes which we do not observe. The reason that we do not see any strong fluctuations as a function of incident energy (which is expected to shift the yields from odd to even isotopes and vice versa) is probably due to the fact that the x rays are still an average over several neighboring odd and even isotopes. In addition, higher compound nucleus angular momenta are reached in our experiment which may result in a noticeable contribution to $\langle M_K \rangle$ from continuum (including statistical) γ-ray transitions. The

use of thin targets in our measurements in contrast to the earlier measurements, allows the evaporation residues to recoil out of the target and our measurements become therefore insensitive to contributions from singular, highly converted low-energy transitions from long-lived states, but rather represent the *average* features of x-ray multiplicities.

A closer inspection of Fig. 11 shows that the multiplicities derived from x-ray—x-ray coincidences are consistently 10–20 % higher than those derived from x-ray and particle singles yields, which may indeed reflect the inequality discussed above. However, within the quoted error limits, we can conclude that our averaging and the assumption of a Poisson multiplicity distribution is justified and the x-ray technique alone can be used to measure multiplicities and cross sections.

For all systems $\langle M_K \rangle$ is a smooth function of energy and varies only slowly over a fairly wide range of energies and ER masses. The strong energy dependence of σ^K, shown in Fig. 4, thus reflects more the energy dependence of the total ER cross sections than that of the multiplicities.

The multiplicities reported here are all of the order of 0.5 to 1; no enhancement of $\langle M_K \rangle$ as found in Li-induced reactions and explained by nuclear structure effects,[11,13] was observed. In fact, the multiplicities are consistent with what one would expect from the conversion of the discrete γ transitions in the cases where they are known, and some contribution from continuum and statistical γ rays. This is inferred, for example, from a comparison of our x-ray multiplicity ($\langle M_K \rangle \simeq 0.7$) for $^{32}S + ^{124}Sn$ at $E_{c.m.} = 100$ MeV with the values from the ^{12}C- and α-induced reactions of Ref. 15. In the latter studies, simultaneous x-ray and γ-ray measurements allowed spectroscopy of individual final evaporation residues and an interpretation of the measured multiplicities ($\langle M_K \rangle \simeq 0.3$–0.4 between ^{151}Dy and ^{153}Dy) in terms of conversion of discrete γ transitions. The difference in multiplicities ($\simeq 0.3$) could be attributed to continuum and statistical γ rays. A discussion of such contributions and their multipolarities is given in Ref. 14.

C. Elemental evaporation residue cross sections

The x-ray multiplicities derived from our x-ray—x-ray coincidence experiments for individual elements (Table II) indicate that $\langle M_K \rangle$ is constant, albeit with large error bars, for the individual ER produced in a given reaction, and we therefore conclude that the relative ER cross sections for the individual elemental channels are represented by the relative K-vacancy production cross sections shown in Fig. 4. The absolute elemental ER cross sections may then be calculated as $\sigma_{Z-i}^{ER} = \langle M_K \rangle \sigma_{Z-i}^{K}$ where $\langle M_K \rangle$ and σ_{Z-i}^{K} are both listed in Table I.

We find that the neutron-rich compound systems decay at lower energies primarily by neutron evaporation leading to Dy isotopes. At higher energies the proton and α (or 2p) evaporation channels leading to Tb and Gd isotopes show increasing strength. For the neutron deficient systems the charge evaporation channels are dominant over

most of the range of incident energies, and for ^{32}S+^{116}Sn we observe almost no evaporation of neutrons only. That α evaporation plays a major role when two or more units of charge have been evaporated may be inferred from the shape of the evaporation residue angular distributions. In Fig. 12 averages of the shapes of the experimental distributions in Fig. 9 have been overlayed at a given incident energy for all Sn targets. In cases where neutron (and thus nucleon evaporation) dominates the shapes are more forward peaked, suggesting that the broadening in cases with multiple charge evaporation is at least partly due to the larger recoil from α particles. The relative strength of the elemental evaporation cross sections can be compared to statistical evaporation calculations using the code CAS-CADE.[23] The basic idea is that a compound nucleus is formed and subsequently, after reaching thermal equilibrium, decays by emission of light particles and γ rays or by fission, with branching ratios as predicted by the statistical theory. Extensive calculations were done on a DEC VAX computer for ^{32}S+^{116,120,124}Sn at 140, 160, and 180 MeV. The theoretical results are normalized to the measured total ER cross sections and plotted as solid-line histograms in Fig. 13. The experimental data appear as full circles with ~20% error bars, which combine statistical errors and systematic errors due to normalization, efficiency calibration and uncertainties in the derivation of $\langle M_K \rangle$ as discussed above. The standard parameter set[23] already leads to a fit that reproduced reasonably well the overall trend, but failed to describe the exact cross sections in many cases. In particular we find that the calculated cross sections are shifted somewhat towards lower-Z residual nuclei, especially for the ^{116}Sn target. A fine tuning of the parameters improved the agreement but some discrepancies still remained. For a meaningful discussion

of the parameter changes which gave the best fit, one has to study the sensitivity of the calculated results to parameter variations. In the first step we adjusted the angular-momentum—dependent effective fission barrier B_f and the level-density parameter ratio a_f/a_n, which determine the fission competition strength. The level density parameter a_n is known to be reasonably well determined by the Fermi gas model[24,25] and a_f often appears to be as much as 25% larger than a_n, which implies that the numbers of levels are greater for the saddle-point configuration than for the ground-state configuration. This reflects the fact that single-particle states have lower energies when the nucleus is well deformed, which leads to a greater number of accessible states in the excited deformed nucleus. In addition, collective states and broken symmetries lead to a further increase of the level density.[26] In order to fit experimental fission cross sections, B_f is often chosen as a fraction of 0.6 to 0.8 of the liquid drop fission barrier. It should be pointed out that B_f and a_f/a_n are not independent variables. We therefore fixed a_f/a_n to 1.0 and adjusted B_f to 0.6 times the liquid drop value in order to match the experimental ratio of the ER cross section to fission cross section at the highest energy (247 MeV), where we have measured the fission cross section.[22] This
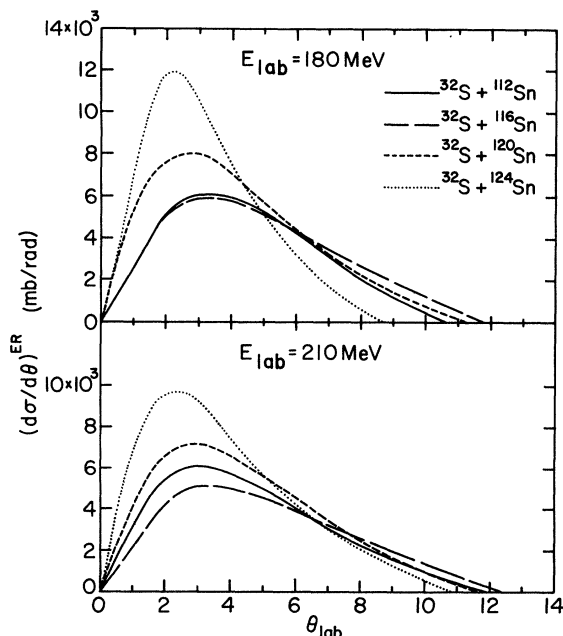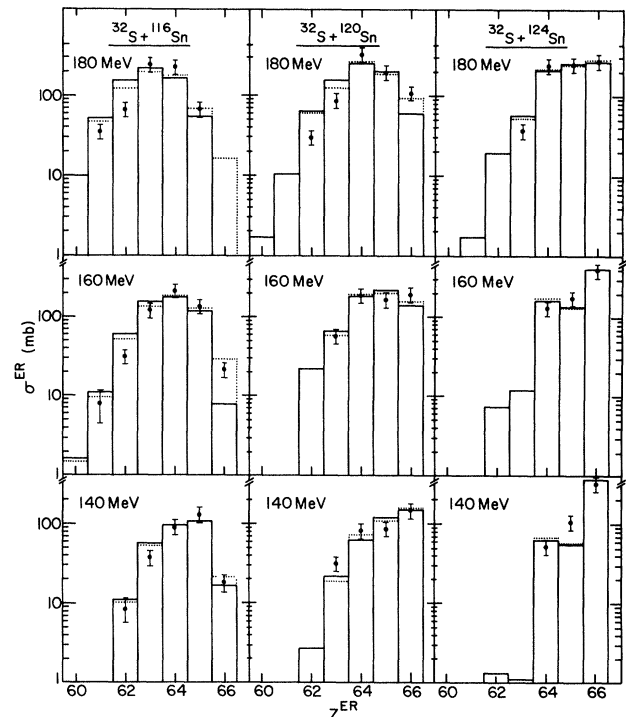

FIG. 13. Comparison of the partial evaporation residue cross sections with statistical-model calculations. The data are indicated as dots, the error bars include both statistical and systematical errors. The full line represents CASCADE (Ref. 23) calculations, the dotted line includes in addition to the CASCADE calculations, an estimate of precompound reactions with the sum rule model (Refs. 30 and 31). In both calculations the total predicted cross section was normalized to the experimentally observed one.

FIG. 12. Comparison of averaged shapes of evaporation residue angular distributions (from Fig. 8) at two incident energies.

choice results in a fission cross section of ~ 80 mb at 160 Mev, which is what one would expect from measurements at comparable energy of similar systems, e.g., $^{35}Cl + {}^{116,124}Sn$.[27]

Most of the parameters of the model, including B_f and a_f/a_n have little influence on the *relative* strength of the elemental cross sections when varied within reasonable limits. Changing a_n between 7 and 9 has, for instance, virtually no effect. We used therefore the standard value $a_n = 8$. The gamma decay strength turned out to be the only really important parameter to have an appreciable influence on the relative Z distribution. We have varied the $E2$ decay strength, neglecting the effects from other multipolarities ($E1$ strength from the giant dipole resonance and possibly $M1$ transitions from shape changes at high spin as observed recently in nuclei near the present mass region[28]; see also our discussion in Sec. IV B). The results are shown in Fig. 14. Increasing the $E2$ strength results in much better fits to the 160-MeV data for $^{32}S + {}^{116}Sn$, where the largest systematic discrepancies occur. For the more neutron-rich systems, where only a few strong channels dominate the ER distribution, the $E2$ strength has less influence. The large $E2$ strength indicates that the compound nuclei exhibit a high collectivity resulting in a large number of fast quadrupole transitions at the excitation energies and angular momenta reached in this experiment. This finding is in line with the large quadrupole components observed recently[29,30] in the continuum γ spectrum of compound nuclei near the present mass region. The $E2$ strength of fast, highly collective $E2$ transitions can reach more than 100 W.u. (Weisskopf units)[30]; on the other hand, since the $E2$ strength is an average over many $E2$ decay paths, which are certainly not all fast, we adopted 50 W.u. as a reasonable maximum value.
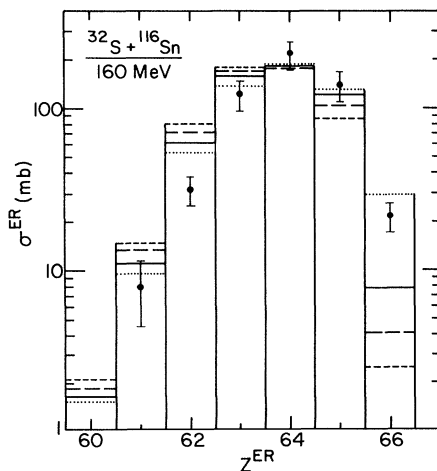

FIG. 14. Comparison of the partial evaporation residue cross sections for 160-MeV $^{32}S + {}^{116}Sn$ with CASCADE (Ref. 23) calculations where the $E2$ transition strength is varied between 50 (solid line), 20 (long-dashed line), and 5 (short-dashed line) W.u. The dotted line represents a CASCADE calculation with an $E2$ strength of 50 W.u. and an additional estimate of precompound light-particle emission cross sections with the sum rule model (Refs. 31 and 32).

However, this value, or even 100 W.u., still did not quite result in a perfect fit to the data. In the next step we included, in addition to n, p, and α evaporation, deuteron evaporation. But it turned out that deuteron evaporation is a very weak channel that can be neglected. There must therefore be an additional degree of freedom which is not included in the statistical model.

One possible explanation could be incomplete fusion or precompound light-particle emission. The statistical treatment of the model assumes that the decay follows an entirely equilibrated ensemble. Any precompound decay prior to equilibration will therefore result in an error. When a light particle is emitted with approximately beam velocity in a precompound process, the residual nucleus remains at a lower excitation energy and angular momentum state as compared to the case of low-velocity emission of the same light particle after equilibration of all degrees of freedom. If this decrease in excitation energy of the residual nucleus is large enough to hinder subsequent charged-particle emission or fission, the statistical model would overestimate multiple charged-particle emission and underestimate the emission of only one neutron, proton, or α particle as compared to the experimentally determined ER cross sections, which may include residues formed in precompound reactions. In order to obtain an estimate of possible precompound contributions, we performed calculations using the sum rule model[31,32] proposed by Wilczyński *et al.* According to this approach the absolute cross sections of all binary reactions which involve an at least partial statistical equilibrium of a strongly interacting dinuclear system can be described by relating the reaction probabilities to the available phase space and to the entrance channel angular momentum limitations. The model has three parameters: an effective temperature T, an effective charge radius parameter r_c, and a diffuseness parameter Δl which describes the smooth cutoff of the transmission coefficients in l space. The model has been applied successfully[32] to the reaction 140-MeV $^{14}N + {}^{159}Tb$.

Since we were only interested in a rough estimate of the precompound contribution, and since the present amount of data does not justify a meaningful fit, we adopted the best-fit values found in Ref. 32 for $^{14}N + {}^{159}Tb$. This system leads to a compound nucleus with an atomic number only 6 units higher than the atomic number of Dy, and with a center-of-mass energy close to that of 160-MeV ^{32}S incident on ^{116}Sn. The resulting cross sections for n, p, and α precompound emission amounted to about 10% of the total ER cross sections and were added to the CASCADE results, which were renormalized such that the sum of both components equaled the experimental total ER cross section. The results appear as dotted histograms in Figs. 13 and 14. For the more neutron-rich targets, where the compound nucleus decay goes through a few strong channels, a weak precompound contribution results only in a minor change of the elemental cross sections, mostly smaller than the experimental errors. But for $^{32}S + {}^{116}Sn$, where the ER spectrum is much broader and the strength of the precompound decay is of the same order as that of some of the elemental ER cross sections, inclusion of

precompound decay leads to a significant improvement (Figs. 13 and 14).

D. Target K-shell ionization cross sections

The characteristic target x rays could, in principle, provide a very convenient way for absolute normalization of ER x-ray cross sections, and replace the most commonly used normalization to the Rutherford cross section of elastically scattered projectiles, measured with a monitor detector. This approach was in fact used by Chmielewska et al.[15] for α-induced reactions, where the theoretical description of atomic target excitation is well developed. But for heavy-ion impact, discrepancies between theory and experiment can be quite large. The semiclassical and nonrelativistic quantum mechanical approaches like the binary-encounter approximation[33] (BEA) and the plane-wave Born approximation[34] (PWBA) tend to increasingly overestimate the cross sections for heavy projectiles. Refined PWBA calculations[35] with perturbation corrections for binding energy distortions of the projectile atomic states and Coulomb deflection of the projectile in the field of the target nucleus (PWBABC) usually give better agreement. The theories are presented in terms of θ, the ratio of the true target K-shell ionization potential I_K to that predicted by hydrogenic wave functions, and by η, the squared ratio of the projectile velocity v to the velocity v_K of the target K electrons:

$$\theta = \frac{I_K}{R_\infty Z_K^2} , \tag{8}$$

$$\eta = \left[\frac{v}{v_K} \right]^2 = \frac{E m_e}{M R_\infty Z_K^2} . \tag{9}$$

E is the projectile energy, M the projectile mass, m_e the electron mass, R_∞ the hydrogen ionization potential (13.6 eV), and $Z_K = Z_t - 0.3$ the effective nuclear charge of the target atoms with atomic number Z_t, as seen by the K electrons. The expressions for the cross sections are then

$$\sigma_{\text{BEA}} = \frac{Z^2}{I_K^2} g(\eta/\theta) , \tag{10}$$

$$\sigma_{\text{PWBA}} = \frac{8\pi Z^2 a_0^2}{Z_K^4} \frac{f(\eta, \theta)}{\eta} , \tag{11}$$

$$\sigma_{\text{PWBABC}} = \frac{8\pi Z^2 a_0^2}{Z_K^4} \frac{F[\eta/(\epsilon\theta)^2]}{\epsilon\theta} C . \tag{12}$$

g (in keV^2 cm^2) is a universal function described in Ref. 33. F and f are dimensionless functions tabulated in Refs. 35 and 34, respectively. The factors ϵ and C provide corrections for the binding energy and the Coulomb deflection effect; they are described in detail in Ref. 35. We have compared our data to these three theories. The predictions of PWBA, BEA, and PWBABC appear as solid lines in Fig. 5. PWBA and BEA overestimate the measured cross sections by about an order of magnitude, while PWBABC gives much better agreement. This tendency has also been observed in other systems.[36]

Another potentially interesting feature of our Sn target x-ray data is the energy dependence of the $K\alpha/K\beta$ intensity ratio. The experimental value for $K\alpha/K\beta$ is 4.55 for the atomic Sn ground-state configuration,[19] while we observe a smooth decrease from 3.74 to 3.25 as the projectile energy is increased, with a tendency to level out at higher energies (Table III and Fig. 6). The reasons for this behavior are higher-shell excitations of the target atom in the same encounter that produced the K vacancy.[33,36] This effect manifests itself also in a slight increase in the centroid energies of the x-ray lines, which was ~ 100 eV in the present case.

For the ER x rays atomic excitation should give only a very small contribution to the observed x-ray yield and multiple excitation should be negligible. In fact, we did not observe a noticeable energy shift of the ER x-ray spectra and, though we could not measure the complete $K\alpha/K\beta$ ratio due to pileup effects as mentioned previously, the $K\alpha_1/K\alpha_2$ ratios, which should also be sensitive to multiple excitation, show no deviations from the ground-state values.

V. CONCLUSIONS

The present study confirms for compound nuclei ($A \gtrsim 150$) formed in reactions with a heavy projectile what was previously observed in reactions with lighter projectiles: Each compound nucleus emits, on the average, approximately one K x ray. The K x rays follow conversion processes that occur during the deexcitation of the evaporation residue after particle evaporation, and are characteristic of the elemental charge Z of that residue. They consequently can yield information about the distribution in Z of the evaporation residues, information not easily obtainable otherwise, since differential energy losses at very low recoil velocities are often in principle not distinguishable. To deduce cross sections from the x-ray yields, the x-ray multiplicity has to be determined. An unambiguous determination is possible in x-ray—γ-ray coincidences with characteristic γ rays of the final evaporation residue. The γ-ray measurements, however, require knowledge of the γ-ray decay schemes which are often not available for proton-rich residual nuclei produced far off the valley of stability in reactions with heavy particles. If γ-ray measurements do allow such identification, the x-ray measurement for cross section determinations are redundant. The x rays are therefore particularly useful for cases where γ-decay schemes are not well known. In such cases x-ray—x-ray coincidences can yield the x-ray multiplicity, if certain assumptions are fulfilled. The present work dealt with this situation and showed that at least for the ^{32}S-induced reactions studied, average multiplicities from x-ray—x-ray coincidences agree well with those deduced from x-ray singles and evaporation residue particle yields. Measurements, and general considerations, on individual Z channels provide results on the distribution of evaporation residues into the various Z channels for several Sn targets and over a large range of incident energies. Statistical-model calculations yield pre-

dictions in rather good agreement with the measured Z distribution of evaporation residues, although some small deviations may be taken as signs of incomplete fusion processes.

This work was supported by the U. S. Department of

*Present address: Physik-Department, Technische Universität München, D-8046 Garching, Federal Republic of Germany.

†Present address: Fermilab, P.O. Box 500, Batavia, IL 60510.

‡Present address: Lawrence Berkeley Laboratory, One Cyclotron Blvd., Berkeley, CA 94720.

[1]W. J. Swiatecki, Phys. Scr. 24, 113 (1981).

[2]A recent review and collection of references is given in L. C. Vaz, J. M. Alexander, and G. R. Satchler, Phys. Rep. 69, 373 (1981).

[3]M. Beckerman, J. Ball, H. Enge, M. Salomaa, A. Sperduto, S. Gazes, A. DiRienzo, and J. D. Molitoris, Phys. Rev. C 23, 1581 (1981).

[4]K.-H. Schmidt, P. Armbruster, F. P. Hessberger, G. Münzenberg, W. Reisdorf, C.-C. Sahm, D. Vermeulen, H.-G. Clerk, J. Keller, and H. Schulte, Z. Phys. A 301, 21 (1981).

[5]W. S. Freeman, H. Ernst, D. F. Geesaman, W. Henning, T. J. Humanic, W. Kühn, G. Rosner, J. P. Schiffer, B. Zeidman, and F. W. Prosser, Phys. Rev. Lett. 50, 1563 (1983).

[6]G. Deconninck and N. Longequeue, Phys. Rev. Lett. 30, 863 (1973).

[7]G. Deconninck and M. Longrée, Phys. Rev. A 16, 1390 (1977).

[8]J. S. Blair, P. Dyer, K. A. Snover, and T. R. Trainor, Phys. Rev. Lett. 41, 1712 (1978).

[9]S. Röhl, S. Hoppenau, and M. Dost, Phys. Rev. Lett. 43, 1300 (1979).

[10]W. E. Meyerhof, R. Anholt, and W. Wölfli, Phys. Lett. 84B, 59 (1979).

[11]H. J. Karwowski, S. E. Vigdor, W. W. Jacobs, S. Kailas, P. P. Singh, F. Soga, and W. D. Ploughe, Phys. Rev. Lett. 42, 1732 (1979).

[12]H. J. Karwowski, S. E. Vigdor, W. W. Jacobs, T. G. Throwe, D. L. Wark, S. Kailas, P. P. Singh, F. Soga, T. E. Ward, and J. Wiggins, Phys. Rev. Lett. 47, 1251 (1981).

[13]H. J. Karwowski, S. E. Vigdor, W. W. Jacobs, S. Kailas, P. P. Singh, F. Soga, T. G. Throwe, T. E. Ward, D. L. Wark, and J. Wiggins, Phys. Rev. C 25, 1355 (1982).

[14]Z. Sujkowski, D. Chmielewska, R. V. F. Janssens, and M. J. A. de Voigt, Phys. Rev. Lett. 43, 998 (1979).

[15]D. Chmielewska, Z. Sujkowski, R. V. F. Janssens, and M. J. A. de Voigt, Nucl. Phys. A366, 142 (1981).

[16]J. Smolorz, S. Hoppenau, S. Röhl, W. A. Schönfeldt, and M. Dost, Phys. Rev. A 21, 207 (1980).

[17]V. Zoran, A. Berinde, C. Deberth, M. Dost, I. O. Neamu, C. Protop, S. Röhl, and N. Scintei, J. Phys. G 6, 117 (1980).

[18]H. Ernst, W. Henning, C. N. Davids, W. S. Freeman, T. J. Humanic, M. Paul, S. J. Sanders, F. W. Prosser, Jr., and R. A. Racca, Phys. Lett. 119, 307 (1982).

[19]W. Bambynek, B. Crasemann, R. W. Fink, H.-U. Freund, H. Mark, C. D. Swift, R. E. Price, and P. V. Rao, Rev. Mod. Phys. 44, 716 (1972).

[20]G. Beier, J. Friese, K. Hartel, P. Kienle, H. J. Körner, Wa. Mayer, L. Müller, K. E. Rehm, W. Scobel, P. Sperr, and W. Wagner, Technical University of Munich Annual Report, 1981.

[21]S. Cohen, F. Plasil, and W. J. Swiatecki, Ann. Phys. (N.Y.) 82, 557 (1974).

[22]H. Ernst, W. Henning, W. S. Freeman, T. J. Humanic, F. W. Prosser, and R. A. Racca (unpublished).

[23]F. Pühlhofer, Nucl. Phys. A280, 267 (1977).

[24]H. Vonach and M. Hille, Nucl. Phys. A127, 289 (1969).

[25]W. Dilg, W. Schantl, H. Vonach, and M. Uhl, Nucl. Phys. A217, 269 (1973).

[26]A. Bohr and B. R. Mottelson, *Nuclear Structure* (Benjamin, New York, 1975), Vol. 2, p. 38.

[27]W. Scobel, H. H. Gutbrod, M. Blann, and A. Mignerey, Phys. Rev. C 14, 1808 (1976).

[28]M. Jääskeläinen, D. G. Sarantites, R. Woodward, F. A. Dilmanian, H. Puchta, J. R. Beene, J. Hattula, M. L. Halbert, D. C. Hensley, and J. H. Barker, Phys. Rev. Lett. 49, 1387 (1982).

[29]P. Chowdhury, J. Borggreen, T. L. Khoo, I. Ahmad, R. K. Smither, S. R. Faber, P. J. Daly, C. L. Dors, and J. Wilson, Phys. Rev. Lett. 47, 778 (1981).

[30]H. Hübel, R. M. Diamond, P. Auger, C. Ellegaard, D. B. Fossan, H. Kluge, C. Schück, S. Shih, F. S. Stephens, and U. Smilanski, Z. Phys. A 304, 225 (1982).

[31]J. Wilczyński, K. Siwek-Wilczyńska, J. van Driel, S. Gonggrijp, D. C. J. M. Hageman, R. V. F. Janssens, J. Lukasiak, and R. H. Siemssen, Phys. Rev. Lett. 45, 606 (1980).

[32]J. Wilczyński, K. Siwek-Wilczyńska, J. van Driel, S. Gonggrijp, D. C. J. M. Hageman, R. V. F. Janssens, J. Lukasiak, R. H. Siemssen, and S. Y. van der Werf, Nucl. Phys. A373, 109 (1982).

[33]J. D. Garcia, R. J. Fortner, and T. M. Kavanagh, Rev. Mod. Phys. 45, 111 (1973).

[34]M. Gryzinski, Phys. Rev. 138, A336 (1965); G. S. Khandelwal, B. H. Choi, and E. Merzbacher, At. Data 1, 103 (1969).

[35]G. Basbas, W. Brandt, and R. Laubert, Phys. Rev. A 7, 983 (1973).

[36]T. J. Gray, P. Richard, R. L. Kauffman, T. C. Holloway, R. K. Gardner, G. M. Light, and J. Guertin, Phys. Rev. A 13, 1344 (1976).